



Promotional effect of Co and Ni on MoO₃ catalysts for hydrogenolysis of dibenzofuran to biphenyl under atmospheric hydrogen pressure



Jie Zhang^a, Chuang Li^a, Weixiang Guan^a, Xiaozhen Chen^a, Xiao Chen^a, Chi-Wing Tsang^b, Changhai Liang^{a,*}

^a State Key Laboratory of Fine Chemicals, Laboratory of Advanced Materials and Catalytic Engineering, School of Chemical Engineering, Dalian University of Technology, Dalian 116023, China

^b Faculty of Science and Technology, Technological and Higher Education Institute of Hong Kong, Hong Kong, China

ARTICLE INFO

Article history:

Received 11 August 2019

Revised 3 January 2020

Accepted 31 January 2020

Keywords:

Hydrogenolysis

Dibenzofuran

Co(Ni)/MoO₃

Biphenyl

Promotional effect

ABSTRACT

Co(Ni)/MoO₃ catalysts were prepared, characterized and evaluated for the hydrogenolysis of bio-derived dibenzofuran (DBF), aiming at the understanding of the promoting effect of Co/Ni on MoO₃ for high-yield production of aromatic products. All Co(Ni)/MoO₃ catalysts selectively cleaved C–O bond, thus effectively transformed DBF to biphenyl (BP) at relatively moderate conditions. The experimental results from varying Mo species by adjusting the reduction temperature of MoO₃ together with XPS and *in-situ* XRD characteristic were evident that Mo⁵⁺ species was responsible as the major active specie for the reaction. Promotional effect between Co(Ni) and Mo in Co(Ni)/MoO₃ catalysts was observed, resulted from the presence of acidic Co(Ni)MoO₄ species and a large number of Mo⁵⁺ species both of which were created local to the Co(Ni)–O–Mo interface, as can be characterized by *in-situ* XRD, XPS, H₂-TPR, NH₃-TPD, *in-situ* FT-IR, Raman and TEM. The trend of the initial reaction rate follows: MoO₃ (0.18 μmol·g_{cat}⁻¹·s⁻¹) < Ni/MoO₃ (0.26 μmol·g_{cat}⁻¹·s⁻¹) < Co/MoO₃ (0.29 μmol·g_{cat}⁻¹·s⁻¹), corresponding to the decreasing activation barrier. And the best catalytic activity was observed for the 100% yield of BP over Co/MoO₃. A possible mechanism, including Co(Ni) facilitated reduction of Mo⁶⁺ to Mo⁵⁺ and Co(Ni) enhanced formation of acidic sites, is proposed to be responsible for the high activity in Co(Ni)/MoO₃ catalysts.

© 2020 Elsevier Inc. All rights reserved.

1. Introduction

The continuous depletion of fossil-fuel, the increasing demand on transportation fuels and the ceaseless deterioration of the environment during these last years arouse a growing need to develop the use of the biomass as potential source for the production of fuels and value-added chemicals [1–5]. However, the high oxygen content of the bio-oil resulting from pyrolysis of biomass, leads to some deleterious properties of the products that include high viscosity, corrosiveness and thermal instability [6,7]. Thus hydrogenolysis is one of the most prevalent and efficient strategies to produce aromatic compounds, which consists of breaking the C–O bond of oxygenated molecules under hydrogen pressure [8]. The process that bio-oil being directly converted into value-added aromatic chemicals, seems to be an attractive route for enhancing the utilization of biomass [3,9,10] with higher efficiency. Thus, during the past several years, catalytic conversion

of biomass-derived model compounds has been extensively studied and the exploration of the reaction mechanisms has provided an insight into effective conversion of bio-oils.

Past efforts for hydrodeoxygenation catalyst development were focused on conventional hydrotreating catalysts, particularly in the petroleum refinery for several decades, such as CoMo- and NiMo-based sulfides [11–16] and supported noble metal catalysts [1,12,17–19]. The sulfided catalysts are active hydrodeoxygenation catalysts, nevertheless, the presence of additional sulfur chemicals for the purpose of avoiding catalyst deactivation results in the inevitable sulfur contamination in the products. Besides, noble metal catalysts could result in full ring saturation, resulting in products with a lower octane number and an increased level of H₂ consumption [20,21]. Thus, more attention has been paid to development of novel catalysts, such as transition metal oxides systems. Recently, metal oxides are considered as more active catalysts capable of C–O bond activation than commonly employed transition metal catalysts [22]. Specifically, molybdenum oxide shows efficient cleavage of C–O bonds on hydrogenation of molybdenum centers [10] under mild conditions, and thus exhibits high selectivity to aromatics for the selective cleavage of C–O bonds in

* Corresponding author.

E-mail address: changhai@dlut.edu.cn (C. Liang).

URL: <http://amce.dlut.edu.cn> (C. Liang).

exploring lignin derivatives upgrading [10,23–25]. Roman-Leshkov et al. demonstrated that MoO_3 effectively catalyzed the hydrogenolysis of lignin-derived oxygenates to produce high yields of aromatic hydrocarbons without ring saturation [26]. It was also reported the selective conversion of guaiacol over MoO_3 to produce various alkylphenols in ethanol without the addition of gaseous hydrogen, with 99% conversion and 94% selectivity of alkylphenols [9]. Moreover, supported MoO_3 catalysts also showed preferable activity of C–O cleavage [4,10,27]. All these important contributions indicate the possibility for MoO_3 to perform excellent ability of C–O cleavage in moderate conditions. However, compared with noble metal catalyst, MoO_3 was relatively less active, and thus the improvement of reactivity was crucial for the development of Mo-based catalyst. Therefore, the rational design of catalysts, which can selectively cleave the C–O bond and improve reaction activity without aromatic saturation under mild conditions, are attracting increasing attention. In previous reports, Co(Ni) as the promoter could significantly enhance the activity of molybdenum sulfide [13], and Co addition to supported molybdenum catalyst enhanced the total hydrodeoxygenation selectivity by 45% in the hydrodeoxygenation of anisole [28]. While, to the best of our knowledge, no systematic studies have been performed to investigate the promotion effect of Co and Ni on MoO_3 catalyst and reaction mechanism for hydrodeoxygenation reactions.

Previous reports have shown that MoO_3 follow a reverse redox reaction mechanism that would result in the removal of the oxygen atom from the oxygenates upon the adsorption of the substrates on the oxygen vacancy sites to form a Mo–O bond with subsequent regeneration of the vacancy with H_2 to produce water [26]. The oxygen in the reactant then fills the oxygen vacancy, leading to oxygen transfer to the catalyst and the formation of the unsaturated product [25,29]. Considering the origin of the catalytic activity of these materials, it is hypothesized that the oxygen vacancy (*i.e.*, an uncoordinated metal site on the metal oxide) is responsible for hydrodeoxygenation over both pure and supported MoO_3 catalysts [25,30,31]. Shanks et al. reported that the MoO_3 catalyst needed to be reduced to a more active form in order to fully deoxygenate the pyrolysis vapors [25]. Therefore, the catalyst requires a constant stream of H_2 for continuous reduction and vacant site formation [25]. Moreover, Roman-Leshkov and co-workers used combined Raman, XRD, and XPS spectroscopy augmented with the deactivation study, to reveal that the activity of MoO_3 could be predominantly promoted by uncoordinated Mo^{5+} species, whereas Mo^{4+} species should be related to the less activity for hydrodeoxygenation reaction [2,21,25,31,32] corresponding to the deactivation reason of MoC_2 that was subsequently transformed to MoO_2 [24]. The above studies suggest the critical role of intermediate state(s) of Mo species on its catalytic performance. Moreover, extensive literatures have been reported on the acidic sites that could also serve as active sites to adsorb the oxygen atom of oxygen-containing compounds and then improve the activity of catalysts [8,33].

In the present work, we select dibenzofuran (DBF) as the lignin model compound [34–38] and focus on the influence of Co(Ni) over MoO_3 on the catalytic activity of catalysts during the hydrogenolysis of DBF to biphenyl at atmospheric hydrogen pressure. First, active sites on pure MoO_3 for the reaction was determined by altering the reduction temperature of MoO_3 to expose the diverse Mo species, combined with the characterization techniques such as XPS and *in-situ* XRD. Then, supported catalysts were synthesized and then used to investigate the activity in order to identify the structural-activity relationship of catalysts as evidenced by *in-situ* XRD, *in-situ* FT-IR, Raman, XPS, H_2 -TPR and NH_3 -TPD. As a result, an insight into a possible reaction mechanism was proposed to illustrate the role of the surface Mo^{5+} and promotional Co(Ni) on catalytic performance over the present catalysts. Developing

mechanistic insights into the active sites of catalysts in the hydrogenolysis of lignin-derived DBF is key to provide new insights for catalyst design and potential applications for bio-oils upgrading.

2. Experimental

2.1. Materials

Ammonium molybdate ($(\text{NH}_4)_6\text{Mo}_7\text{O}_{24}\cdot 4\text{H}_2\text{O}$, $\geq 99.0\%$), cobalt nitrate ($\text{Co}(\text{NO}_3)_2\cdot 6\text{H}_2\text{O}$, $\geq 98.5\%$) and nickel nitrate ($\text{Ni}(\text{NO}_3)_2\cdot 6\text{H}_2\text{O}$, $\geq 98.0\%$) were obtained from Sinopharm Chemical Reagent Co. Methanol (CH_3OH , 99.8%) and *n*-decane ($\text{C}_{10}\text{H}_{22}$, 98%) were purchased from Tianjin Kermel Chemical Reagent Co. Dibenzofuran ($\text{C}_{12}\text{H}_8\text{O}$, 98.0%) and *n*-dodecane ($\text{C}_{12}\text{H}_{26}$, 99.0%) were obtained from Aladdin Chemical Reagent Co. All of the materials were analytical reagent grade and utilized without further purification.

2.2. Preparation of catalysts

MoO_3 was prepared by calcining $(\text{NH}_4)_6\text{Mo}_7\text{O}_{24}$ under Ar/O_2 (40/20 mL min^{-1}) flow at 500 °C for 4 h. 3 wt% Co(Ni)/ MoO_3 were prepared by the wetness impregnation method with methanol solution of $\text{Ni}(\text{NO}_3)_2$ or $\text{Co}(\text{NO}_3)_2$. Typically, a certain amount of $\text{Ni}(\text{NO}_3)_2\cdot 6\text{H}_2\text{O}$ or $\text{Co}(\text{NO}_3)_2\cdot 6\text{H}_2\text{O}$ was dissolved in 60 mL methanol at room temperature and then 2.00 g MoO_3 was added under vigorous stirring for 8 h. After that, methanol was removed using a rotary evaporator at 40 °C and the slightly damp sample was dried overnight at 80 °C. Finally, the samples were calcined at 400 °C for 4 h under Ar/O_2 (40/20 mL min^{-1}) flow for further characterization and catalytic measurements. Co(Ni) MoO_4 were prepared using a precipitation method described in detail in the [Supporting Information](#).

MoO_3 reduced at different temperature were denoted as MoO_{3-n} ($n = 300, 400, 500$ and 600 °C). In addition, MoO_3 , Ni/ MoO_3 and Co/ MoO_3 represented catalysts reduced at 300 °C.

2.3. Characterization of catalysts

2.3.1. Nitrogen adsorption

N_2 adsorption–desorption isotherms of the catalysts were measured at -196 °C using a Quantachrome Autosorb IQ instrument. Prior to these measurements, the sample was loaded in a glass tube and outgassed at 200 °C under vacuum for 8 h to remove any volatile adsorbates from the surface. The resulting adsorption isotherms were used to calculate the specific surface area (*S*) by the Brunauer-Emmett-Teller (BET) method. The average pore volume (V_p) and the pore diameter (d_p) was obtained using the Barrett-Joyner-Halenda (BJH) method.

2.3.2. In-situ X-ray diffraction

In-situ X-ray diffraction (XRD) patterns were recorded on a Rigaku Smartlab instrument, using a Cu $K\alpha$ monochromatized radiation source. Diffraction patterns were collected in the range of 2 θ from 5° to 90° with a scan speed of 8° min^{-1} , operated at 40 kV and 100 mA. Prior to test, the samples were placed into the reaction chamber and reduced in flowing H_2 (40 mL min^{-1}) at corresponding temperature for 2 h, and then the diffraction patterns were collected.

2.3.3. Temperature-programmed desorption

The acidic properties of catalysts were characterized by using the temperature-programmed desorption of ammonia (NH_3 -TPD). Experiments were performed on a CHEMBET-3000 chemisorption instrument. Prior to the experiments, the calcined samples

(0.10 g) were pre-reduced with 10% H₂/He at 400 °C for 2 h at a heating ramp rate of 10 °C min⁻¹. After pretreatment, the temperature was cooled to 120 °C and the sample was saturated with a 10% NH₃/He stream for 1 h. After removing physically adsorbed NH₃ by purging with He at 120 °C for 1 h, the samples were heated to 500 °C at a heating rate of 10 °C min⁻¹ in a He flow. The amount of acidic sites on the catalyst was calculated from the desorption amount of NH₃, which was determined by measuring the areas of the desorption profiles.

2.3.4. In-situ Fourier transform infrared spectra

Fourier transform Infrared (FT-IR) spectra was collected at room temperature on a Thermo Fisher iN10 spectrometer with a resolution of 4 cm⁻¹ for 16 scans in the region 400–4000 cm⁻¹. The pellets were prepared by mixing 10 mg of sample in 150 mg KBr and then placed into an *in-situ* environmental cell. Afterward, the samples were heated from 30 °C to 300 °C with a ramp rate of 5 °C min⁻¹ and maintained for 2 h in 40 mL min⁻¹ H₂ flow. After the reactor was cooled to room temperature, H₂ was switched to He with a total flow rate of 40 mL min⁻¹ for 20 min and then the spectra were recorded.

2.3.5. Raman spectroscopy

Raman spectra was recorded at room temperature on a Thermo Scientific DXR Raman Microscope (Renishaw England) equipped with a liquid-nitrogen cooled charge coupled device (CCD) detector and a confocal microscope. The line at 532 nm Ar laser was used as excitation source and the scanning range was 50–3500 nm⁻¹. The laser was focused on the sample under a microscope with the diameter of the analyzed spot being ~1 μm. The wavenumber values reported are accurate to within 2 cm⁻¹.

2.3.6. X-ray photoelectron spectroscopy

X-ray photoelectron spectra (XPS) was measured using a photoelectron spectrometer (ESCALAB250) with a monochromatic Al Kα X-ray source (1486.6 eV, operating at 15 kV and 20 mA). The binding energy was preliminarily calibrated using the peak positions of the adventitious carbon (C 1s, 284.6 eV). The composition of Mo oxidation states was estimated by the deconvolution of Mo 3d doublet. Relative element concentrations were determined by the integral areas of the core-level spectra. After background subtracted by the Shirley method, the spectra were fitted into several peaks using a convolution of Gaussian and Lorentzian functions.

2.3.7. Scanning electron microscope

Scanning electron microscope (SEM) images of the samples were obtained on a FEI Nova Nano SEM 450 electron microscope with a voltage in the range of 0.5–30 kV. The results were discussed in supporting information (Figs. S1 and S2).

2.3.8. Transmission electron microscopy

Transmission electron microscopy (TEM) was performed on a Philips CM 120 instrument operated at 120 keV. Samples were dispersed ultrasonically in ethanol and deposited on a copper grid and dried at room temperature.

2.3.9. Temperature programmed reduction

Temperature programmed reduction (H₂-TPR) measure was carried out on AutoChem II 2920 Chemisorption Analyzer with a thermal conductivity detector (TCD). 50 mg of fresh sample was loaded in an isothermal zone of a quartz U-tube reactor and heated from 30 °C to 300 °C with a ramp rate of 10 °C min⁻¹ and maintained for 2 h in 30 mL min⁻¹ Ar gas, which facilitates desorption of the physically adsorbed water. After the reactor was cooled to room temperature, Ar was switched to 10% H₂ in Ar at a total flow rate of 30 mL min⁻¹ and the temperature was linearly raised to

900 °C at a continuous heating ramp of 5 °C min⁻¹. The response of the detector was recorded by gas chromatograph using the TCD.

2.3.10. Elemental analysis (ICP-AES)

The elemental composition of as-prepared catalysts was measured by means of inductively coupled plasma atomic emission spectroscopy (ICP-AES) on a Perkin-Elmer Optima 2000 DV device.

2.4. Catalytic activity

The hydrogenolysis of DBF was performed in a vapor-phase down-flow fixed-bed reactor, as described in our previous works [8,38]. The temperature inside the reactor was monitored by a K-type thermocouple extended into the catalyst bed. The catalyst (0.40 g) was diluted with 60–80 mesh quartz SiO₂ (5 mL) to keep the catalyst bed isothermal. Prior to catalytic tests, all the synthesized catalysts were reduced in fixed-bed reactor at different temperature (300 °C, 400 °C, 500 °C and 600 °C) and 1.0 MPa for 2 h with a hydrogen flow rate of 40 mL min⁻¹. Then, the temperature and pressure of the reactor were adjusted to reaction conditions (0.1 MPa H₂ pressure and 360 °C). The reactants consisted of 2.0 wt% DBF, 1.0 wt% *n*-dodecane (as an internal standard), and 97.0 wt% *n*-decane (as solvent), were fed into the reactor from the top of the reactor by a pump along with H₂ gas. The mixture of reactant and H₂ gas moved downward and reacted in the middle of the reactor. Catalytic tests were conducted until reaching the steady state. The Weighted Hourly Space Velocity (WHSV, h⁻¹) was calculated from the catalyst weight and the reactant flow as defined as follows:

$$\text{WHSV} = (g_{\text{DBF}}/h)/g_{\text{catalyst}} \quad (1)$$

The feed and the reaction products were analyzed off-line by an Agilent gas chromatograph 7890A equipped with a flame ionization detector (FID) and a 0.5 μm × 0.32 mm × 30 m FFAP capillary column. The products were determined by GC-MS with an Agilent 7890B with 5977A MSD and a 0.25 μm × 0.25 mm × 30 m HP-5 capillary column.

The conversion (X) of DBF and the selectivity (S_i) of products were defined as follows:

$$X = \frac{n_0 - n_{\text{DBF}}}{n_0} \times 100\% \quad (2)$$

$$S_i = \frac{n_i}{\sum n_i} \times 100\% \quad (3)$$

where n₀ and n_{DBF} define the moles of DBF in the feed and product, respectively, n_i denotes the mole of product i and ∑n_i are the total moles of products.

The carbon balance of products was within ±5% with no gas generated.

$$\text{Carbon balance}(\%) = \frac{\text{moles of carbon of all products}}{\text{moles of carbon of reactant fed}} \quad (4)$$

The reaction rate (μmol·g_{cat}⁻¹·s⁻¹) was calculated at low conversion based on the formula.

$$\text{The reaction rate} = \frac{F_{\text{WDBF}}X}{M_{\text{DBF}}W} = \frac{W_{\text{DBF}}X}{M_{\text{DBF}}\tau} \quad (5)$$

where W_{DBF} denotes the weight fraction of DBF in the reactant and M_{DBF} denotes the molecular mass of DBF.

3. Results and discussion

3.1. Determination of the active sites on pure MoO₃ catalyst.

Considering the complexity of valence states of Mo, MoO₃ at different reduction temperature which were exposed as varying Mo species, were selected as the catalyst to better determine the nature of the active sites (Fig. 1). On an equivalent Mo mass basis, the conversions over MoO₃ at different reduction temperature exhibited a considerable discrepancy, in which MoO₃-300 catalyst reached the best activity. At the reduction temperature of 300 °C, the conversion increased from 75% to 83% at 0.13 g_{DBF}/g_{catalyst}·h, followed by a reduction with further increase in reduction temperature of MoO₃. However, the selectivity toward deoxygenated product (BP) remained at 100% over all MoO₃ catalysts even with lower WHSV (not shown), which was inconsistent with our previous results over supported noble metals [38,39]. This indicated that the hydrogenolysis of DBF does not produce the *o*-phenylphenol (OPP) by just cleaving one C-O bond and thus Mo species could facilitate the direct removal of oxygen atom in DBF.

To determine the nature of the active sites, *in-situ* XRD and XPS were used. *In-situ* XRD patterns of MoO₃ catalysts reduced at different temperature (300, 400, 500 and 600 °C) are shown in Fig. 2. First of all, it can be seen that synthetic MoO₃ presented the characteristic peaks of the MoO₃ crystalline phase (PDF#35-0609), which suggested that pure MoO₃ was obtained and the structure was consistent with the orthorhombic molybdenum trioxide. At the reduction temperature of 300 °C, no obvious disparity was found in reduced MoO₃ compared to unreduced MoO₃. When the temperature was increased to 400 °C, the new peaks at 26° and 37° appeared, which indicated that a little MoO₂ has been formed based on the comparison of the observed XRD peak intensities from both MoO₃ and MoO₂ phases. The peak intensity of MoO₃ decreased obviously as temperature was increased. Further increasing the temperature to 500 °C, the major phase had been changed to MoO₂ (PDF#32-0671). When the temperature was increased to 600 °C, almost all species were transformed into metal Mo⁰.

XRD did not specifically distinguish the change of the surface Mo species of MoO₃ at the reduction temperature of 300 °C and 400 °C. The chemical state of the Mo species in catalyst surface played an important role in the oxygen-removal reaction. Therefore, XPS spectra was used to investigate the nature of the surface Mo species [12]. Prior to any deconvolution of the XPS data, it is already evident that all catalyst samples contain a significant fraction of Mo⁶⁺ species in the form of MoO₃ (Fig. 3). After deconvolu-

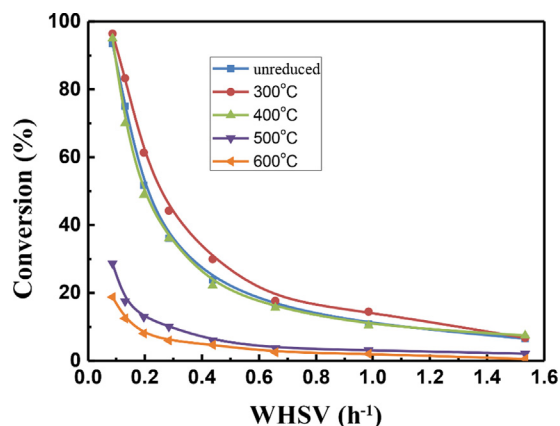


Fig. 1. Hydrogenolysis conversion of DBF as a function of WHSV (g_{DBF}/g_{catalyst}·h) using MoO₃ catalysts reduced at 300, 400, 500 and 600 °C for 2 h.

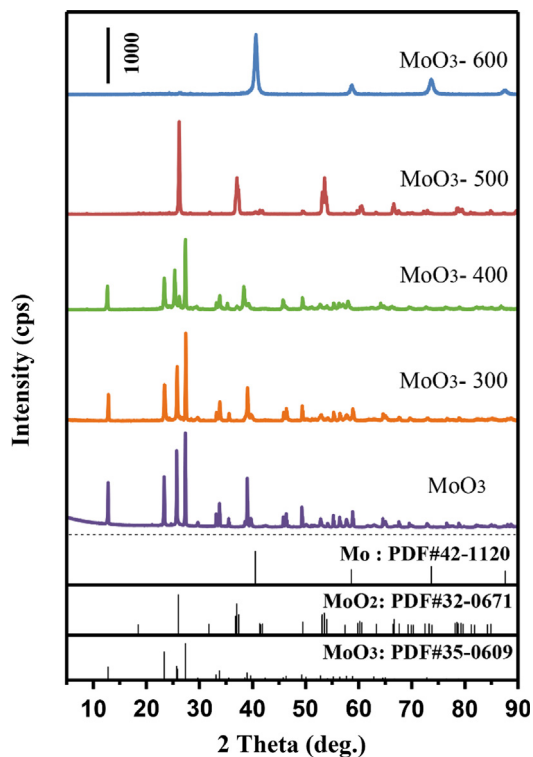


Fig. 2. *In-situ* XRD patterns of MoO₃ catalysts reduced at different temperature for 2 h.

tion of the XPS spectra, the contribution of the various Mo species such as Mo⁶⁺, Mo⁵⁺, Mo⁴⁺ has been calculated (Table 1). Mo⁵⁺ species was observed in a mild reduction of MoO₃ at 300 °C (Fig. 3a). With further reduction of MoO₃ at 400 °C, in addition to the peak of Mo⁵⁺ surface species, peaks corresponding to Mo⁴⁺ also appeared (Fig. 3b). Previous DFT calculations suggested that a portion of the surface oxygen of MoO₃ can be removed to generate oxygen vacancy sites [26] at 400 °C, even though the partial reduction to form uncoordinated metal sites was undetectable by XRD.

The specific surface area of calcined MoO₃ (17 m² g⁻¹) is very low as shown in Table 2, and then thus the change of surface area of MoO₃ at different reduction temperature should not result in such a considerable difference in activity, thereby confirming that the hydrogenolysis activity arose from the Mo species, as characterized by XRD and XPS. In comparison with pure MoO₃, as the proportion of Mo⁵⁺ slightly increased, there existed an increasing trend in catalytic activity. When reduction temperature was increased, the presence of Mo⁴⁺ species reduced the catalytic performance. Further increasing the temperature up to 500 °C led to the formation of the major phase MoO₂ and thus a sharp decrease in the activity occurred, suggesting that MoO₂ is an inactive phase for the reaction which was in agreement with previous reports [2,24,31]. Additionally, as reduction further proceeded, the generated Mo⁰ showed lower activity than MoO₂. Hence, the creation of strong Mo active sites for the removal of oxygen were highly dependent on the reduction temperature by H₂ pre-treatment and thus influenced the activity of the catalyst. These observed results suggested that uncoordinated Mo sites had a significant impact on the conversion of dibenzofuran and the extent of the effect follows: Mo⁵⁺ > Mo⁶⁺ >> Mo⁴⁺ > Mo⁰.

The results demonstrated that surface oxygen vacancies derived from Mo⁵⁺ play a central role in the HDO of dibenzofuran. In the next step, we selected 300 °C as the reduction temperature of the catalyst and focused on understanding the role of Co(Ni) in

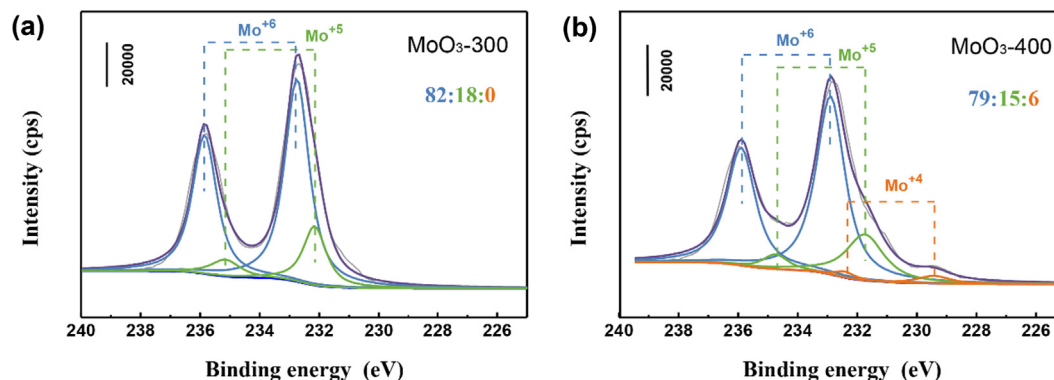


Fig. 3. XPS spectra of the Mo (3d) energy region in MoO₃ reduced at 300 °C (a) and 400 °C (b). The ratios displayed correspond to the proportion of oxidation states of Mo⁶⁺, Mo⁵⁺ and Mo⁴⁺.

Table 1

The proportion of different Mo species from the XPS.

Sample	The proportion of different Mo species (%)		
	Mo ⁶⁺	Mo ⁵⁺	Mo ⁴⁺
MoO ₃ -300	82	18	0
MoO ₃ -400	79	15	6
Co/MoO ₃ ^a	42	56	2
Ni/MoO ₃ ^b	58	23	19

^{a,b} Catalysts reduced at 300 °C for 2 h.

enhancing the hydrogenolysis rate of MoO₃ during the hydrogenolysis reaction at atmospheric H₂ pressure.

3.2. Interaction of Co(Ni) and MoO₃

The Co(Ni)/MoO₃ catalysts were extensively characterized to explore the interaction between Co(Ni) and MoO₃. Temperature-programmed reduction with hydrogen (H₂-TPR) was used to assess the interaction between the metal and the support (Fig. 4). The TPR profile of pure MoO₃ showed two major peaks at 639 and 699 °C corresponding to the reduction of MoO₃ to MoO₂, and one minor reduction peak at 756 °C corresponding to conversion of MoO₃ to Mo₄O₁₁ [2,40]. The further reduction of MoO₂ to Mo occurred at about 1000 °C (not shown) [40]. These reduction process were consistent with previous study using *in-situ* XAFS and XRD [41]. For Co (Ni)/MoO₃ catalysts, the reduction peaks in the range of 400–699 °C were observed, which can be associated with the reduction process of octahedrally coordinated Mo⁶⁺ presented in MoO₃ and Co(Ni)MoO₄ to Mo⁴⁺ [21,28,42,43], in which the peak at 464 °C for the Ni/MoO₃ belonged to the reduction of nickel oxide [44,45]. The peak at 355 °C for the Co/MoO₃ was attributed to the reduction of Co₃O₄ to CoO [28,46,47]. And the peak of further reduction of CoO to Co may have overlapped with that corresponding to the reduction of MoO₃ at 450–500 °C [47]. Higher temperature (~800 °C) was attributed to further reduction of MoO₂ species formed in the first reduction process at 644 °C [42]. Compared to MoO₃ sample spectra, the H₂-TPR of Co(Ni)/MoO₃ catalysts proved

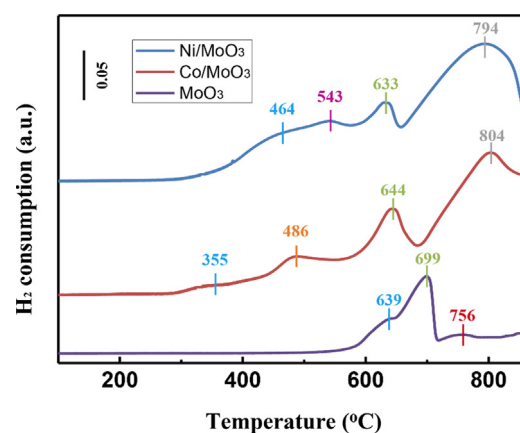


Fig. 4. H₂-TPR for the calcined MoO₃ and Co(Ni)/MoO₃ catalysts.

that the addition of Co(Ni) appeared to increase the reducibility of the MoO₃ species. The main peak at 699 °C on MoO₃ corresponding to the reduction of MoO₃ to MoO₂ shifted to lower temperatures (633 and 644 °C) with the respective addition of Ni and Co. Besides, Ni had a stronger promotion on the reducibility of the MoO₃ species than Co. These observations were consistent with previous report, showing that the reduction of metal oxides was facilitated by the presence of the other adjacent metal considering the reducibility of the catalysts [48]. It should be noted that the concentration of hydrogen in H₂-TPR is far less than that in prior pre-treatment reaction and thus H₂-TPR was just used to compare the reducibility of catalysts.

In-situ XRD was used to further assess the effect of Co(Ni) on the reducibility of MoO₃ in Fig. 5. In contrast to the XRD results with the standard PDF card of MoO₃, it was obvious that all the catalysts showed a typical MoO₃ pattern. XRD did not identify the presence of oxidized Co(Ni) on the calcined catalysts resulting from the corresponding impregnation of MoO₃ with the cobalt or nickel salt, an observation that could be explained by the fact that only a small

Table 2

The catalytic performance of MoO₃ and Co(Ni)/MoO₃ catalysts at WHSV of 0.13 g_{DBF}/g_{catalyst}·h.

Samples	S ^a (m ² g ⁻¹)	Initial reaction rate (μmol·g ⁻¹ ·s ⁻¹)	Conversion (%)	BP selectivity (%)	The amount of acidity ^b (mmol g ⁻¹)	Mo ⁵⁺⁶ (%)	E _a (kJ mol ⁻¹)
MoO ₃	17	0.18	83	100	0.004	18	152
Co/MoO ₃	11	0.29	97	100	0.048	56	131
Ni/MoO ₃	11	0.26	91	86	0.056	23	140

^a Determined using calcined samples.

^{b,c} Determined using reduced samples at 300 °C for 2 h.

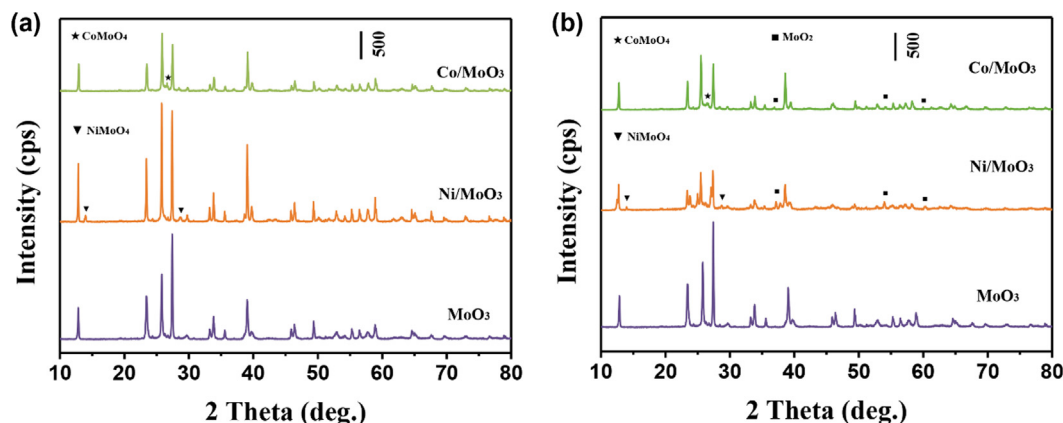


Fig. 5. *In-situ* XRD patterns of MoO₃ and Co(Ni)/MoO₃ catalysts at (a) oxidation states and (b) reduction states (reduction at 300 °C for 2 h).

amount of modifier was added. However, the new peaks of Co/MoO₃ ($2\theta = 25.2^\circ$) and Ni/MoO₃ ($2\theta = 14.3, 28.5^\circ$) were detected at oxide states compared with MoO₃, suggesting cobalt molybdate and nickel molybdate were formed [28,49]. And the cobalt/nickel molybdate still existed under the present reduction conditions. Furthermore, the peak intensity of MoO₃ decreased obviously on MoO₃ modified by Co(Ni), and the peaks of MoO₂ appeared, which demonstrated that the reduction of MoO₃ is facilitated by the presence of the Co(Ni) [48] and this was consistent with H₂-TPR results. Moreover, Ni-modified MoO₃ was more prompt to be reduced than that modified with Co due to the fact that the peak intensity of MoO₂ in Ni/MoO₃ was much stronger than Co/MoO₃ (Fig. 5b), as also evidenced by H₂-TPR.

XPS was carried out to identify the chemical states of Mo species (Fig. 6). The surface fraction of Mo⁵⁺ predominantly increased along with the addition of Co(Ni) compared with MoO₃ catalyst, indicating the addition of Co (Ni) could accelerate the reduction process from Mo⁶⁺ to Mo⁵⁺. However, Ni also promotes the reduction of Mo⁵⁺ to Mo⁴⁺ as well as Mo⁶⁺ to Mo⁵⁺ due to the stronger promotion to MoO₃ reduction as proved by XRD and H₂-TPR. It seems that Co prevented over-reduction to lower oxidation states compared to Ni species.

The preceding characterization had been shown that the Co(Ni) can promote the reduction of MoO₃. Further, temperature programmed desorption with ammonia (NH₃-TPD) was performed to determine the total amounts of acid centers as well as their acid strength of the three catalysts (Fig. 7a). The corresponding values ($\mu\text{mol g}^{-1}$) were listed in Table 2. The reduced MoO₃ was found to have few acidity which was consistent with the results reported

by Shanks and coworkers, in which the fresh MoO₃ was found to contain some acidity, whereas by reducing the catalyst at 350 °C for one hour, the acidity greatly diminished as compared with the fresh catalyst [25]. It can be concluded that the addition of Co(Ni) could significantly increase the acidity of catalyst, and the explanation for this may be related to the formation of Co(Ni)MoO₄ considering the lesser acidity of metal Co(Ni), as evidenced by NH₃-TPD of CoMoO₄ (Fig. S4).

To explore the acidic sites, Raman spectroscopy was used to determinate the formation of Co(Ni)MoO₄ (Fig. 7b). The band at 998 cm⁻¹ can be assigned to the terminal (Mo-O) stretching vibrations [21,42,43,49,50]. The band at 820 cm⁻¹ can be attributed to the antisymmetric (Mo-O-Mo) stretching modes [21,42]. The band centered at 673 cm⁻¹ is due to an asymmetric stretching of the Mo-O-Mo [42]. The band at 292 cm⁻¹ belongs to a doublet comprised of wagging modes of the terminal oxygen connected to Mo atoms [42]. The Raman spectra of Co/MoO₃ sample not only possessed the characteristic peaks of MoO₃, but also presented new bands at about 692 and 938 cm⁻¹, which stood for the main bands of CoMoO₄ [48,51]. In addition, the Raman spectra of Ni/MoO₃ sample exhibited additional band of NiMoO₄ at about 963 cm⁻¹ [49]. Raman spectroscopic data of the catalysts showed a superficial interaction between Co(Ni) and Mo in catalysts calcined at 400 °C, probably with the formation of Co(Ni)-O-Mo phases presented in the surface.

Apart from the characterization of Raman, the Co(Ni)MoO₄ species was also proved by the *in-situ* FT-IR (Fig. 7c). Three types of connections between Mo and O atoms were presented [21,49,52]. The broad and complex band centered at about 625 cm⁻¹ is due

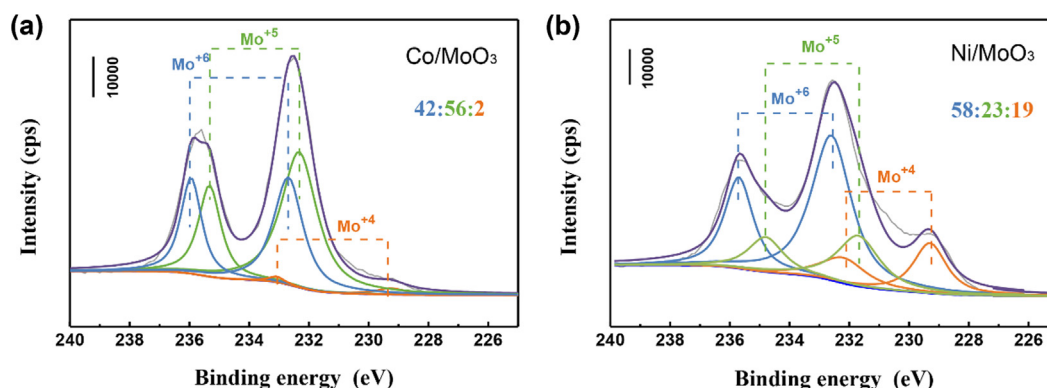


Fig. 6. X-ray photoelectron spectra (XPS) of the Mo (3d) energy region in Co/MoO₃ (a) and Ni/MoO₃ (b) catalysts reduced at 300 °C for 2 h. The ratios displayed correspond to the proportion of oxidation states of Mo⁶⁺, Mo⁵⁺ and Mo⁴⁺.

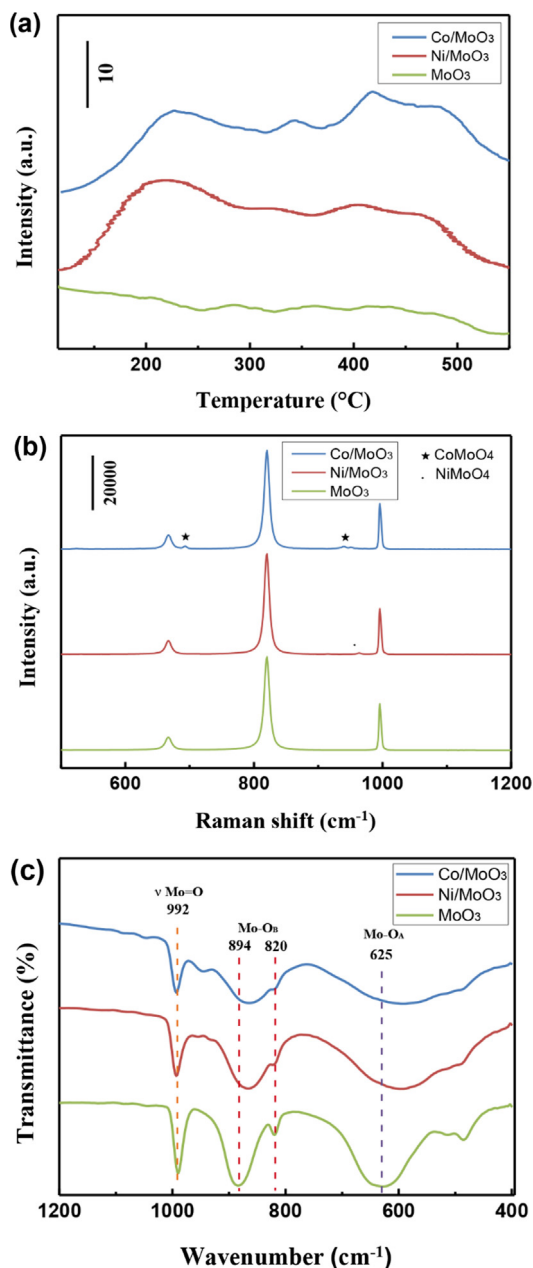


Fig. 7. (a) NH_3 -TPD, (b) Raman spectra and (c) *in-situ* FT-IR spectra of MoO_3 and Co(Ni)/MoO_3 catalysts reduced at 300°C for 2 h.

to the stretching vibration of the O_A atoms each linked to three Mo atoms. The two absorption patterns at 820 cm^{-1} and 894 cm^{-1} could be attributed to the vibration of the O_B atoms in Mo-O-Mo entities. A band at 992 cm^{-1} was attributed to the vibration of the terminal oxygen in Mo-O. The bands corresponding to O_A stretching modes shifted to lower wavenumber with the addition of Co(Ni) , as evidenced by the shifting of the band at 625 cm^{-1} for MoO_3 to 594 cm^{-1} for Co/MoO_3 and Ni/MoO_3 . Furthermore, the band at 894 cm^{-1} corresponding to O_B stretching modes also shifted to lower wavenumber. The position of terminal Mo-O and the band at 820 cm^{-1} , however, was not significantly affected. Note that there was a strong absorption band at 945 cm^{-1} over Co/MoO_3 , assigned to CoMoO_4 species, which was typical of the octahedral configuration of Mo [52]. These results elucidated that Co(Ni) could interact with Mo- O_A and Mo- O_B and then the new species Co(Ni)MoO_4 were formed, which was also evidenced by XRD (Fig. 4) and Raman spectroscopy (Fig. 7b).

The combined characterization of NH_3 -TPD, Raman and *in-situ* FT-IR confirmed that Co(Ni)MoO_4 were the acidic sites of catalysts. To further visually demonstrate the presence of acidic site, TEM was used to probe the Co/MoO_3 catalyst. The obtained Co/MoO_3 was nanosheet (Fig. 8a). HRTEM further showed existence of CoMoO_4 with the interplanar distance of 0.33 nm , which corresponded to the $(0\ 0\ 2)$ plane (Fig. 8b).

On the basis of the above results, the addition of Co(Ni) promotes the reduction of MoO_3 and the generation of acidic Co(Ni)MoO_4 species, thus increases the active sites of catalysts.

3.3. The role of Co(Ni) on the hydrogenolysis of dibenzofuran

The catalysts were tested for the hydrogenolysis activity and the results were shown in Fig. 9. In general, strong promotional effect was observed, and Co/MoO_3 was observed to have a stronger promotional effect than Ni/MoO_3 , which was consistent with the previous report[53]. The initial reaction rate was increased from $0.18\ \mu\text{mol}\cdot\text{g}_{\text{cat}}^{-1}\cdot\text{s}^{-1}$ (MoO_3) to $0.29\ \mu\text{mol}\cdot\text{g}_{\text{cat}}^{-1}\cdot\text{s}^{-1}$ (Co/MoO_3) and $0.26\ \mu\text{mol}\cdot\text{g}_{\text{cat}}^{-1}\cdot\text{s}^{-1}$ (Ni/MoO_3). The promotional effects observed can be explained by an increase of the number of active sites. BP was the major product with the selectivity of 95% over Ni/MoO_3 and 100% over MoO_3 and Co/MoO_3 . As the WHSV decreased, the BP selectivity was gradually decreased over Ni/MoO_3 accompanied by an increased selectivity to cyclohexylbenzene (Fig. S5), whereas the BP selectivity over Co/MoO_3 still maintained at 100%, due to the higher hydrogenation activity of Ni than Co [16,54]. The apparent activation energy (E_a) of catalysts was calculated (Fig. S6) and the results were shown in Table 2. The addition of Co(Ni) could lead to a decrease in the activation barrier of hydrogenolysis of DBF and further result in an increase in the reaction activity. These results showed that MoO_3 promoted by Co(Ni) could catalyze the oxygen-removal reactions with high efficiency.

3.4. Determination of the active sites on Co(Ni)/MoO_3

To determine the active sites for the Co(Ni)/MoO_3 catalysts, the studies on reaction rates as a function of acidic sites, active Mo^{5+} species, could provide an in-depth understanding of active centers and their individual contribution toward the reaction. The activity of Co(Ni)/MoO_3 catalysts reduced at different reduction temperature was explored in order to expose the varying quantity of acidic sites and Mo^{5+} species (Table S2, Figs. S7–S9). In this study, the increase of reaction rates and acidity was not a linear relationship over Co(Ni)/MoO_3 catalysts (Figs. S10a and S11a), illustrating that acidic sites serve as the active site but not an exclusive factor to govern catalytic performance. Furthermore, it should be mentioned that the Mo species in Co(Ni)/MoO_3 also strongly affect the reaction rates of catalysts (Figs. S10b and S11b). These results suggest that the hydrogenolysis activity of DBF is not only associated with the acidic sites, but also related to the Mo species of catalysts.

3.4.1. Role of the Mo^{5+} species on Co(Ni)/MoO_3

The experimental results from varying Mo species by adjusting the reduction temperature of MoO_3 have already confirmed that the presence of these different Mo species demonstrated a significant effect on the catalytic performance and Mo^{5+} species and this could be responsible for the improved activity, as determined by the relationship between the reaction results and the characterization results (XRD and XPS). With the addition of Co(Ni) to MoO_3 , the reaction rate distinctly increased with the increase in Mo^{5+} species (Table 2), indicating that Mo^{5+} species of Co(Ni)/MoO_3 played an important role for the reaction and Co(Ni) facilitated the reduction process from Mo^{6+} to Mo^{5+} . Further, the experimental results from exposing different amounts of Mo^{5+}

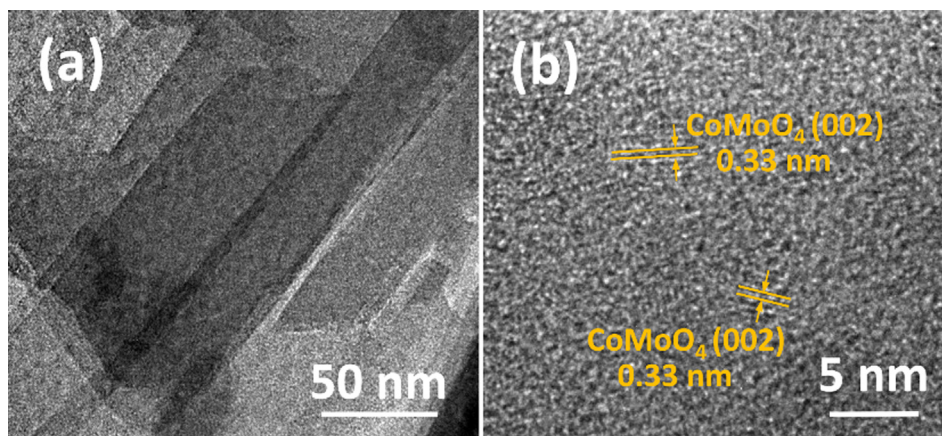


Fig. 8. TEM images (a and b) of Co/MoO₃ reduced at 300 °C for 2 h.

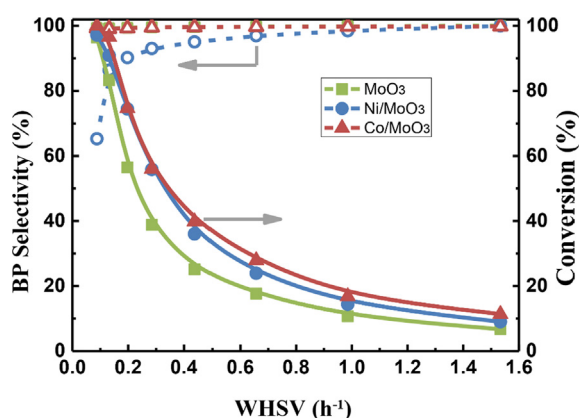


Fig. 9. BP selectivity and conversion as a function of WHSV ($g_{\text{DBF}}/g_{\text{catalyst}} \cdot \text{h}$) during the hydrogenolysis of DBF over MoO₃ and Co(Ni)/MoO₃ reduced at 300 °C for 2 h.

species by changing the reduction temperature of Co(Ni)/MoO₃ indicated that the Mo⁵⁺ species is the one active site for the reaction (Fig. S10b).

Regarding the reducibility of the catalysts, the existence of a synergetic effect between Co(Ni) and Mo should be noted since the reduction of metal oxides was facilitated by the presence of the other adjacent metal. XRD and XPS showed that the addition of Co(Ni), even in very small amount, could increase the reducibility of MoO₃ species and thus increase the amount of Mo⁵⁺. The prevalence of Mo⁵⁺ species, indicative of the creation of active defects, arose from the reduction of MoO₃ to MoO_{3-x} [27]. Previous report proposed that the promoter (Ni and Co) can donate electrons to molybdenum and lead to a weakening of the metal-sulfur bond of MoS₂, resulting in an increase in the number of vacancy sites [16]. Tran et al. also reported that cobalt not only facilitated the reduction and dispersion of nickel oxide but also enhanced the HDO activity of bimetallic Ni-Co catalyst [54]. Similarly, the Pd could facilitate reduction of Fe oxide based on H₂-TPR studies and DFT calculations [55]. Indeed, interaction of Co(Ni) and Mo also promotes the reduction of molybdenum oxides [56]. It was shown that an oxygen atom between two molybdenum atoms is less strongly bonded than an oxygen atom bonded between a nickel (or cobalt) and a molybdenum atom and can be more easily removed (Fig. S3), thus creating a vacancy, which was different from the promotional effect of Co(Ni) on MoS₂, albeit both enhance reaction rate by creating a larger number of vacancy [57].

3.4.2. Role of the acidic sites on Co(Ni)/MoO₃

The addition of Co(Ni) increased the acidity of the catalysts in comparison to MoO₃ with no acidity (Fig. 7a), along with the formation of Co(Ni)MoO₄ species, as characterized by the Raman (Fig. 7b) and FT-IR (Fig. 7c) spectroscopies. The NH₃-TPD profiles of synthetic CoMoO₄ further confirmed that the acidic sites were derived from the formation of CoMoO₄ species (Fig. S4), and previous report [58] also verified the acidity of Co(Ni)MoO₄. Moreover, the Co(Ni) species of Co(Ni)MoO₄ were more difficult to be reduced than those of Co(Ni)/MoO₃ (Fig. S3), which was in agreement with previous report [58], thereby it may indicate the possibility of the existence of Co(Ni)MoO₄ in our pre-treatment condition, which are in accord with the preceding results.

The synthetic Co(Ni)MoO₄ samples were used as the catalysts in an attempt to investigate the influence of acidic sites on the reaction activity. The Co(Ni)MoO₄ showed a similar conversion as the MoO₃ (~25%), both of which were lower than the conversion of Co(Ni)/MoO₃ (~40%) (Table S3). It indicated that the high activities of Co(Ni)/MoO₃ could result from the synergistic effect between Mo species and the acidic sites rather than a single effect. In the Co(Ni)MoO₄, the Mo atoms were more difficult to be reduced than the Co atoms, as evidenced by TPR (Fig. S3), hence unsaturated Mo was not the main contributor to the activity of the corresponding catalysts. In order to exclude the effect of Mo species, the reaction rate per unit mole of Mo was calculated (Table S3). The reaction rates of CoMoO₄ and NiMoO₄ (1.17 and 1.07 $\mu\text{mol} \cdot \text{mol}_{\text{Mo}}^{-1} \cdot \text{s}^{-1} \cdot 10^2$, respectively) were far more than MoO₃ (0.66 $\mu\text{mol} \cdot \text{mol}_{\text{Mo}}^{-1} \cdot \text{s}^{-1} \cdot 10^2$), which showed that acidic sites would be of great importance in the reaction and the activity was significantly increased regardless of the activity of Mo species. The experimental results from changing the amounts of acidic sites by increasing the reduction temperature of Co(Ni)/MoO₃ further indicated that the acidic sites are the active sites for the reaction (Figs. S10a and S11a). Subsequently, it can be concluded that the high activities of Co(Ni)/MoO₃ catalysts were the results of the synergistic effect between Mo species and acidic Co(Ni)MoO₄ species.

3.5. Reaction mechanism

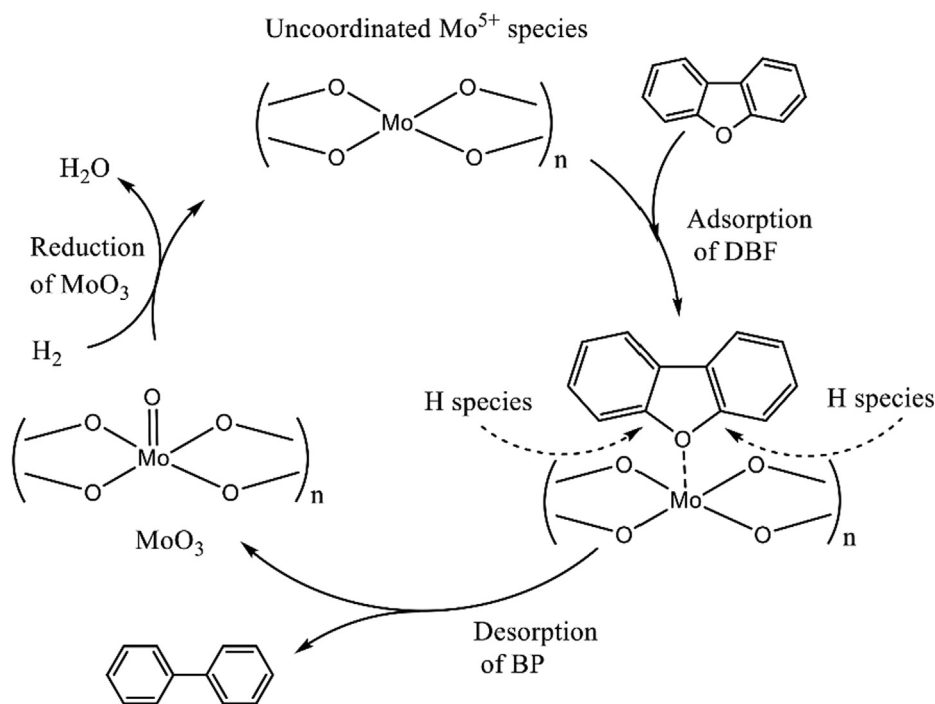
First of all, the reaction mechanism of pure MoO₃ catalyzing the cleavage of C-O bond should be proposed. The reduced MoO₃ has no acidity, as evidenced by NH₃-TPD (Fig. 7a), which elucidated that the cleavage of C-O bond was not going through acid-base catalytic mechanism. On the other hand, as described in Section 3.1, the results demonstrated that unsaturated Mo⁵⁺ species were the major active species for MoO₃. Therefore, surface oxygen vacancy

derived from unsaturated Mo^{5+} played a pivotal role in the HDO of dibenzofuran. It was well accepted that oxygen-removal reaction involves an oxygen vacancy mechanism over MoO_3 catalysts [4,25,26]. This reaction mechanism shown in Scheme 1 had the following elementary reaction steps (1), (2) and (3): (1) in the initial induction period, MoO_3 was reduced by H_2 as a reductant to form adequate number of Mo^{5+} sites for reactions; (2) oxygen atoms of dibenzofuran molecules interacted with Mo^{5+} sites to form Mo-O bond, followed by cleavage of the C-O bond; (3) sequential desorption of the formative BP occurred. Eventually, H_2 reduced the already-oxidized catalyst surface to expose the active sites again [26].

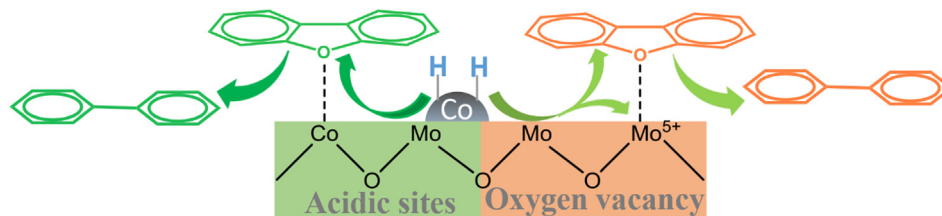
Next, the reaction mechanism of Co(Ni)/MoO_3 was discussed. In Co(Ni)/MoO_3 catalysts, the metallic Co(Ni) species were observed, as evidenced by the XPS (Fig. S12) and TPR (Fig. 4), which may be associated with the activation of hydrogen and enrichment of the surface hydrogen populations. The presence of $\text{Co}^{2+}/\text{Ni}^{2+}$ in XPS also confirmed the formation of Co(Ni)MoO_4 species and it can be difficult to be reduced in current conditions (Fig. S12). Metallic Co(Ni) species were capable for H_2 activation and increased availability of reactive hydrogen surface to aid in the removal of oxygen [59]. However, Bartholomew stated that the kinetics and energetics of hydrogen adsorption on cobalt and nickel were significantly changed by metal-support interactions, particularly in catalysts of low metal content or involving highly reducible supports [60]. Prins proposed that hydrogen spillover occurred mainly in the reducible oxides because the defect sites can stabilize atomic hydrogen [61], hence the reducible MoO_3 may provide the possibility for hydrogen spillover. The activated hydrogen species on Co(Ni) can spill over and migrate onto the MoO_3 surface. The reduction of Mo^{6+} to Mo^{5+} species promoted by the addition of Co(Ni) may be enhanced by means of hydrogen spillover that can be improved by the increased acidity [8,62], which corresponds well with the increase of acidity of catalysts. However, H species by spillover do not travel much further than the immediate interface between the metal particle and the metal-oxide support [61]. Therefore, the oxygen atoms at the

boundary region of metal particle and oxide support, can be more easily removed by an adsorbed H species, leaving behind an oxygen vacancy [63]. It also indicated that the metal-support interfaces provide a chance for the hydrogen spillover and may be the area where most of the H atoms react with DBF to generate BP on the interface.

The addition of Co(Ni) could increase the number of Mo^{5+} sites and promote the formation of Co(Ni)MoO_4 species, both of which were the active sites for the reaction. It should be noted that the oxophilic Mo species could increase the interaction of the surface with oxygen-containing functional groups [64]. Resasco et al. also demonstrated that the metal oxophilicity makes the direct cleavage of the C-O bond in the surface easier [65]. Additionally, it was known that the acidic sites of catalyst could accelerate the adsorption of oxygen-containing compounds [8,66]. During the deoxygenation of benzyl alcohol, the Mo species could cause the aromatic ring to repel from the surface, resulting in alteration of the adsorption orientation as well as a reduction of the adsorption strength, as evidenced by the DFT calculation and experiment studies [67]. These indicated that the DBF molecules were favorable to be adsorbed on the catalyst surface by the interaction between the oxygen atom of DBF and two types of active sites in non-coplanar manner, which may be one reason why smaller hydrogenated product was observed. As previously indicated, the HDO of DBF over Co(Ni)/MoO_3 occurred both through the oxygen vacancies and the acidic sites. Moreover, the HDO reaction may also involve the enhanced hydrogen spillover by acidic sites of Co(Ni)/MoO_3 catalysts and the hydrogen by spillover could promote the cleavage of C-O bond adsorbed on Mo^{5+} species and acidic sites. The supposed schematic of the C-O hydrogenolysis mechanism of DBF over Co/MoO_3 catalyst was illustrated with Scheme 2. The dissociated hydrogen on the metallic Co(Ni) in metal-support interface was provided by the spillover for the unsaturated Mo^{5+} sites and acidic sites where the DBF molecules can adsorb and activate. The reasons for the much higher activity of Co(Ni)/MoO_3 than the MoO_3 catalyst included the increased hydrogen species promoted by Co(Ni) , the higher rate of reduction



Scheme 1. Supposed schematic of the C-O hydrogenolysis mechanism of DBF over Co/MoO_3 catalyst.



Scheme 2. Supposed schematic of the C-O hydrogenolysis mechanism of DBF over Co/MoO₃ catalyst.

from Mo⁶⁺ to Mo⁵⁺ species assisted by Co(Ni) and finally, the effective formation of acidic sites. The results thus may act as a guidance for future designing of highly active and selective deoxygenation catalyst for conversion of lignin.

4. Conclusion

The results from varying the nature of Mo species by adjusting the reduction temperature of MoO₃ and the characterization of these species by XPS and *in-situ* XRD strongly supported that Mo species had a significant impact on the conversion of dibenzofuran and the extent of the effect follows: Mo⁵⁺ > Mo⁶⁺ >> Mo⁴⁺ > Mo⁰. A strong promotional effect in activity between Co(Ni) and Mo in Co(Ni)/MoO₃ catalysts was observed, which was resulted from specific Co(Ni)-Mo interaction in which Co(Ni) facilitated the reduction from Mo⁶⁺ to Mo⁵⁺ species and the formation of acidic Co(Ni)MoO₄ species, as evidenced by *in-situ* XRD, XPS, H₂-TPR, NH₃-TPD, Raman, *in-situ* FT-IR and TEM. Ni/MoO₃ showed a lower activity than Co/MoO₃, which was related to the further reduction of Mo⁵⁺ to Mo⁴⁺ species, and the observation of aromatic hydrogenation ring on Ni/MoO₃, both of which may be due to the higher ability to dissociate hydrogen molecules on Ni. Except for Ni/MoO₃, all catalysts were capable of exhibiting remarkable selectivity for C-O bond cleavage without hydrogenation of aromatic rings, giving striking biphenyl selectivity of 100% at relatively moderate conditions. The best catalytic activity was realized over Co/MoO₃ with a 100% yield of BP, which might be related to the interaction of Co and Mo species as reflected by the decreased activation energy. A possible mechanism, including Co(Ni) facilitated reduction of Mo⁶⁺ to Mo⁵⁺ and Co(Ni) enhanced formation of acidic sites, was proposed to be responsible for the high activity and BP selectivity in Co(Ni)/MoO₃ catalysts.

Declaration of Competing Interest

The authors declare that they have no known competing financial interests or personal relationships that could have appeared to influence the work reported in this paper.

Acknowledgements

This work was financially supported by the National Key Research & Development Program of China (2016YFB0600305). The authors thank Instrumental Analysis & Research Center for their analysis assistance.

Appendix A. Supplementary material

Supplementary data to this article can be found online at <https://doi.org/10.1016/j.jcat.2020.01.035>.

References

- [1] J. He, C. Zhao, D. Mei, J.A. Lercher, *J. Catal.* 309 (2014) 280–290.
- [2] M. Shetty, K. Murugappan, T. Prasomsri, W.H. Green, Y. Román-Leshkov, *J. Catal.* 331 (2015) 86–97.

- [3] J.N. Chheda, G.W. Huber, J.A. Dumesic, *Angew. Chem. Int. Ed.* 46 (2007) 7164–7183.
- [4] V.O.O. Gonçalves, C. Ciotonea, S. Arrii-Clacens, N. Guignard, C. Roudaut, J. Rousseau, J.-M. Clacens, S. Royer, F. Richard, *Appl. Catal. B* 214 (2017) 57–66.
- [5] A.M. Robinson, J.E. Hensley, J.W. Medlin, *ACS Catal.* 6 (2016) 5026–5043.
- [6] D.P. Serrano, J.A. Melero, G. Morales, J. Iglesias, P. Pizarro, *Catal. Rev.* 60 (2017) 1–70.
- [7] A.N.K. Lup, F. Abnisa, W.M.A.W. Daud, M.K. Aroua, *Appl. Catal. A* 541 (2017) 87–106.
- [8] J. Zhang, C. Li, X. Chen, Y. Chen, L. Zhang, B. Zhang, C. Liang, *J. Catal.* 371 (2019) 346–356.
- [9] K. Cui, L. Yang, Z. Ma, F. Yan, K. Wu, Y. Sang, H. Chen, Y. Li, *Appl. Catal. B* 219 (2017) 592–602.
- [10] L.P. Xiao, S. Wang, H. Li, Z. Li, Z.-J. Shi, L. Xiao, R.C. Sun, Y. Fang, G. Song, *ACS Catal.* 7 (2017) 7535–7542.
- [11] A.L. Jongorius, R. Jastrzebski, P.C.A. Bruijninx, B.M. Weckhuysen, *J. Catal.* 285 (2012) 315–323.
- [12] G.D.L. Puente, J.J.P.A. Gil, P. Grange, *Langmuir* 15 (1999) 5800–5806.
- [13] V.N. Bui, D. Laurenti, P. Afanasiev, C. Geantet, *Appl. Catal. B* 101 (2011) 239–245.
- [14] A.E. Coumans, E.J.M. Hensen, *Appl. Catal. B* 201 (2017) 290–301.
- [15] A. Popov, E. Kondratieva, L. Marley, J.M. Goupil, J. El Fallah, J.-P. Gilson, A. Travert, F. Maugé, *J. Catal.* 297 (2013) 176–186.
- [16] Y. Romero, F. Richard, S. Brunet, *Appl. Catal. B* 98 (2010) 213–223.
- [17] M. Grilc, B. Likozar, *Chem. Eng. J.* 330 (2017) 383–397.
- [18] Z. Strassberger, A.H. Alberts, M.J. Louwerse, S. Tanase, G. Rothenberg, *Green Chem.* 15 (2013) 768.
- [19] F. Yang, D. Liu, H. Wang, X. Liu, J. Han, Q. Ge, X. Zhu, *J. Catal.* 349 (2017) 84–97.
- [20] G.W. Huber, S. Iborra, A. Corma, *Chem. Rev.* 106 (2006) 4044–4098.
- [21] M. Shetty, K. Murugappan, W.H. Green, Y. Román-Leshkov, *A.C.S. Sustain. Chem. Eng.* 5 (2017) 5293–5301.
- [22] K.A. Goula, A.V. Mironenko, G.R. Jenness, T. Mazal, D.G. Vlachos, *Nat. Catal.* 2 (2019) 269–276.
- [23] S. Boulloua-Eiras, R. Lødeng, H. Bergem, M. Stöcker, L. Hannevold, E.A. Blekkan, *Catal. Today* 223 (2014) 44–53.
- [24] P.M. Mortensen, H.W.P. de Carvalho, J.-D. Grunwaldt, P.A. Jensen, A.D. Jensen, *J. Catal.* 328 (2015) 208–215.
- [25] M.W. Nolte, J. Zhang, B.H. Shanks, *Green Chem.* 18 (2016) 134–138.
- [26] T. Prasomsri, T. Nimmanwudipong, Y. Román-Leshkov, *Energ. Environ. Sci.* 6 (2013) 1732.
- [27] C. Ranga, R. Lødeng, V.I. Alexiadis, T. Rajkhowa, H. Bjørkan, S. Chytil, I.H. Svenum, J. Walmsley, C. Detavernier, H. Poelman, P. Van Der Voort, J.W. Thybaut, *Chem. Eng. J.* 335 (2018) 120–132.
- [28] C. Ranga, V.I. Alexiadis, J. Lauwaert, R. Lødeng, J.W. Thybaut, *Appl. Catal. A* 571 (2019) 61–70.
- [29] T.M. Sankaranarayanan, A. Berenguer, C. Ochoa-Hernández, I. Moreno, P. Jana, J.M. Coronado, D.P. Serrano, P. Pizarro, *Catal. Today* 243 (2015) 163–172.
- [30] T. Prasomsri, M. Shetty, K. Murugappan, Y. Román-Leshkov, *Energ. Environ. Sci.* 7 (2014) 2660–2669.
- [31] K. Murugappan, E.M. Anderson, D. Teschner, T.E. Jones, K. Skorupska, Y. Román-Leshkov, *Nat. Catal.* 1 (2018) 960–967.
- [32] C. Bouchy, C. Pham-Huu, B. Heinrich, C. Chaumont, M.J. Ledoux, *J. Catal.* 190 (2000) 92–103.
- [33] F. Hoxha, B. Schimmoeller, Z. Cakl, A. Urakawa, T. Mallat, S.E. Pratsinis, A. Baiker, *J. Catal.* 271 (2010) 115–124.
- [34] J.A. Cecilia, A. Infantes-Molina, E. Rodríguez-Castellón, A. Jiménez-López, S.T. Oyama, *Appl. Catal. B* 136–137 (2013) 140–149.
- [35] Y. Wang, Y. Fang, T. He, H. Hu, J. Wu, *Catal. Commun.* 12 (2011) 1201–1205.
- [36] H.W. Lee, B.R. Jun, H. Kim, D.H. Kim, J.-K. Jeon, S.H. Park, C.H. Ko, T.W. Kim, Y.K. Park, *Energy* 81 (2015) 33–40.
- [37] D. Ballesteros-Plata, A. Infantes-Molina, M. Rodríguez-Cuadrado, E. Rodríguez-Aguado, P. Braos-García, E. Rodríguez-Castellón, *Appl. Catal. A* 547 (2017) 86–95.
- [38] J. Zhang, C. Li, X. Chen, W. Guan, C. Liang, *Catal. Today* 319 (2019) 155–163.
- [39] J. Zhang, L. Wang, C. Li, S. Jin, C. Liang, *Org. Process Res. Dev.* 22 (2018) 67–76.
- [40] K.R.R. Thallada Bhaskar, Chinthala Praveen Kumar, Mamidanna R.V.S. Murthy, Komandur V.R. Chary, *Appl. Catal. A* 211 (2001) 189–201.
- [41] R.E.J.T. Ressler, J. Wienold, M.M. Gunter, O. Timpe, *J. Phys. Chem. B* 104 (2000) 6360–6370.
- [42] Y. Cui, N. Liu, Y. Xia, J. Lv, S. Zheng, N. Xue, L. Peng, X. Guo, W. Ding, *J. Mol. Catal. A* 394 (2014) 1–9.
- [43] T. Hahn, U. Bentrup, M. Armbrüster, E.V. Kondratenko, D. Linke, *ChemCatChem* 6 (2014) 1664–1672.

- [44] S. Jin, Z. Xiao, C. Li, X. Chen, L. Wang, J. Xing, W. Li, C. Liang, *Catal. Today* 234 (2014) 125–132.
- [45] E. Heracleous, A. Lee, K. Wilson, A. Lemonidou, *J. Catal.* 231 (2005) 159–171.
- [46] H. Song, L. Zhang, U.S. Ozkan, *Green Chem.* 9 (2007) 686–694.
- [47] R. Nava, B. Pawelec, P. Castaño, M.C. Álvarez-Galván, C.V. Loricera, J.L.G. Fierro, *Appl. Catal. B* 92 (2009) 154–167.
- [48] C.P. Cheng, G.L. Schrader, *J. Catal.* 60 (1979) 276–294.
- [49] L.M. Madeira, M.F. Portela, C. Mazzocchia, *Catal. Rev.* 46 (2004) 53–110.
- [50] J. Jiao, J. Fu, Y. Wei, Z. Zhao, A. Duan, C. Xu, J. Li, H. Song, P. Zheng, X. Wang, Y. Yang, Y. Liu, *J. Catal.* 356 (2017) 269–282.
- [51] X. Xia, W. Lei, Q. Hao, W. Wang, X. Wang, *Electrochim. Acta* 99 (2013) 253–261.
- [52] C.A.C. Mazzocchia, C. Diagne, E. Tempesti, J.M. Herrmann, G. Thomas, *Catal. Lett.* 10 (1991) 181–192.
- [53] T. Klicpera, M. Zdražil, *J. Catal.* 206 (2002) 314–320.
- [54] N.T.T. Tran, Y. Uemura, S. Chowdhury, A. Ramli, *Appl. Catal. A* 512 (2016) 93–100.
- [55] Y. Hong, H. Zhang, J. Sun, K.M. Ayman, A.J.R. Hensley, M. Gu, M.H. Engelhard, J. S. McEwen, Y. Wang, *ACS Catal.* 4 (2014) 3335–3345.
- [56] R.G. Kukushkin, O.A. Bulavchenko, V.V. Kaichev, V.A. Yakovlev, *Appl. Catal. B* 163 (2015) 531–538.
- [57] M. Egorova, R. Prins, *J. Catal.* 225 (2004) 417–427.
- [58] N.F.Y.-S. Yoon, W. Ueda, Y. Moro-oka, K.-W. Lee, *Catal. Today* 24 (1995) 327–333.
- [59] M. Pozzo, D. Alfè, *Int. J. Hydrogen Energ.* 34 (2009) 1922–1930.
- [60] C.H. Bartholomew, *Catal. Lett.* 7 (1990) 27–52.
- [61] R. Prins, *Chem. Rev.* 112 (2012) 2714–2738.
- [62] Y. Liu, J. Zhao, Y. He, J. Feng, T. Wu, D. Li, *J. Catal.* 348 (2017) 135–145.
- [63] P.S. Antonio Ruiz Puigdollers, Sergio Tosoni, Gianfranco Pacchioni, *ACS Catal.* 7 (2017) 6493–6513.
- [64] A. Robinson, G.A. Ferguson, J.R. Gallagher, S. Cheah, G.T. Beckham, J.A. Schaidle, J.E. Hensley, J.W. Medlin, *ACS Catal.* 6 (2016) 4356–4368.
- [65] Q. Tan, G. Wang, A. Long, A. Dinse, C. Buda, J. Shabaker, D.E. Resasco, *J. Catal.* 347 (2017) 102–115.
- [66] A. Popov, E. Kondratieva, J.M. Goupil, L. Mariey, P. Bazin, J.-P. Gilson, A. Travert, F. Mauge, *J. Phys. Chem. C* 114 (2010) 15661–15670.
- [67] A.M. Robinson, L. Mark, M.J. Rasmussen, J.E. Hensley, J.W. Medlin, *J. Phys. Chem. C* 120 (2016) 26824–26833.